Ecological Engineering 181 (2022) 106677

Contents lists available at ScienceDirect

Ecological Engineering

journal homepage: www.elsevier.com/locate/ecoleng

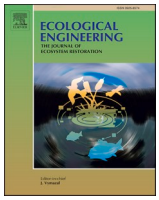

Novel indices for snow avalanche protection assessment and monitoring of wind-disturbed forests

Tommaso Baggio [a,*], Natalie Brožová [b,c,d], Alexander Bast [b,d], Peter Bebi [b,d], Vincenzo D'Agostino [a]

[a] Department of Land, Environment, Agriculture and Forestry, University of Padova, Legnaro, Italy
[b] Alpine Environment and Natural Hazards, WSL Institute for Snow and Avalanche Research SLF, Davos Dorf, Switzerland
[c] Department of Environmental Systems Science, Swiss Federal Institute of Technology (ETH Zurich), Zurich, Switzerland
[d] Climate Change, Extremes and Natural Hazards in Alpine Regions Research Center CERC, Davos Dorf, Switzerland

ARTICLE INFO

Keywords:
Windthrow
Spatial indices
Snow avalanche
Protection forest
Natural hazard assessment

ABSTRACT

Windstorms are natural disturbances predicted to increase in frequency in the future, with a consequent increased risk of damage to forests. Such damage severely affects the forest structure and, therefore, its protection capacity. Previous studies analyzed post event conditions and the recovery time of abated forest within study areas smaller than 10 ha, while not accounting for larger spatial scales. In this study, we propose a new methodology to provide tools for the spatial assessment and monitoring of protection forests against snow avalanches affected by large-scale windstorms. Four indices have been used: (i) vegetation height model, (ii) surface roughness, (iii) stored volume height and (iv) adapted tree parameters, of which the latter two have been specifically developed for this goal. We selected and periodically recorded two windthrow areas using photogrammetric surveys (deriving dense point clouds) to assess the performance of the proposed indices and to investigate the long-term changes in protective effects (Disentis, CH) and the influence of snow cover (Franza, IT). Stored volume height and the adapted tree parameters were the best indices to capture the forest conditions and standing trees, respectively. The stored volume height was further used to estimate forest protective capacity in relation to the snow cover height. Analyzing the Disentis (CH) area, we concluded that the minimum level of protective capacity occurs ten years after the storm event. After 29 years, the forest protective capacity against natural hazards increased again as forest recovery proceeded. However, special attention should be given to gaps between growing trees that may be critical for potential avalanche formation as wood decays. This study provided new insights into the long-term protective efficiency of windthrow forests, introducing two new indices to spatially assess and monitors their evolution.

1. Introduction

Protection forests are forested areas with designated protective functions against natural hazards (Brang et al., 2001). In the Alpine region, forests protect against different gravitational hazards, such as snow avalanches, rockfalls, shallow landslides and debris flows (Getzner et al., 2017). Protection forests stabilize the soil and reduce surface runoff, limiting sediment transport (Chandler et al., 2018; Hegg et al., 2005) and the runout distance of mass flow phenomena (May, 2002; Michelini et al., 2017). Regarding snow avalanches, forests reduce the formation of homogeneous snowpack and the potentially weak layers with altered microclimates (Moeser et al., 2015) and stabilize snowpack using the tree stems (McClung and Schaerer, 2006). In the case of rockfall, trees and shrubs reduce the runout distance and bounce height of falling rocks (Dorren et al., 2005; Rammer et al., 2015).

However, once protection forests are significantly disturbed, their protective function may decrease or become eliminated if the forest is severely disturbed (Berger and Rey, 2004). As a result, disturbed forests may not provide sufficient protection against cascading effects. A study of the remaining postdisturbance protective effects and the time of forest recovery is therefore of fundamental importance to adequately assess the protective function over time. Furthermore, since forest disturbances are expected to increase in the future due to climate change (Allan et al., 2021; Seidl et al., 2017), the interactions between natural hazards and

* Corresponding author.
E-mail address: tommaso.baggio@unipd.it (T. Baggio).

https://doi.org/10.1016/j.ecoleng.2022.106677
Received 28 December 2021; Received in revised form 22 April 2022; Accepted 1 May 2022
Available online 12 May 2022

disturbed forests will be a topic of high relevance in mountainous regions (Bebi et al., 2017; Paine et al., 1998). Wildfires, snow avalanches, shallow landslides, insect outbreaks and storms are common natural disturbances for European forests may affect extensive areas of protection forests. In particular, storms with critical wind speeds produce severe and extended damage to European forests (Gardiner et al., 2010; Schiesser et al., 1997; Seidl et al., 2014b). Such storms have shown an increasing trend in frequency and magnitude in recent decades due to legacies of former land use and climate change (Gardiner et al., 2010; Seidl et al., 2011). A good example is the Vaia storm that occurred in October 2018, which is considered one of the largest wind disturbances observed on the southern side of the European Alps in recent times (Motta et al., 2018).

After a windthrow event, fallen trees can provide residual protection against natural hazards (Schönenberger, 2002a). Such protection gradually decreases due to breakage processes and wood decay (Wohlgemuth et al., 2017). The remaining standing trees together with advanced regeneration play a fundamental role in starting natural regeneration (Seidl et al., 2014a). After a certain period, new trees can provide efficient protection against natural hazards. Between biomass degradation and the establishment of new trees, a minimum protection capacity may occur (Wohlgemuth et al., 2017). Identification of the residual protective capacity and its temporal evolution together with natural regeneration are major processes for hazard evaluation and management of disturbed forests in populated mountain areas. The assessment of residual protection, the time of minimum level of protection and the period of forest recovery is particularly significant in the case of protection forests against snow avalanches affected by disturbance. Some studies have investigated the avalanche protection of wind-disturbed forests through aerial and field data (Schönenberger et al., 2005; Wohlgemuth et al., 2017). They analyzed the damaged tree characteristics (dislocation of lying trunks, log stability and stem height above ground) and the regeneration rate (sapling density, species composition and protection efficacy) in a maximum period of 24 years since the windstorm at different sites in the Swiss Alps. The results reported a considerably small number of observed snow avalanches and rockfall events, while a higher frequency of shallow landslides and debris flows has been recorded (Bebi et al., 2019; Wohlgemuth et al., 2017). The reported studies investigated the changes in different forest parameters for areas smaller than 10 ha (Schönenberger, 2002a, 2002b). The logistics of continuous sampling in the field over longer periods are time-consuming and cost ineffective. Furthermore, the accessibility to disturbed forests is demanding, especially over large areas. A spatial quantification method applicable at a regional scale to assess disturbed forest temporal development for snow avalanche protection over larger areas is still lacking.

The spatial quantification of the protection capacity of forest biomass disturbed by a storm event is of crucial importance for hazard mapping since pre-event forests can have different stand characteristics (density, basal area, mean height, species composition, etc.). On the other hand, forests with the same characteristics could be affected by storms in separate ways depending on the prevailing wind direction and local topography. The resulting irregular surface is characterized by spaces between trees where a variable snow volume could be stored, contributing to snow cover stabilization and avoiding the formation of weak layers and therefore hindering the release of snow avalanches. In this context, some studies reported the analysis of windthrow areas mainly based on field surveys. Even if these data are of high interest for the hazard assessment of similar windthrow forests, civil authorities and practitioners can benefit from the development of spatial indices that can be applicable over large areas (greater than 10 ha) and based on remotely sensed data such as LiDAR or photogrammetric surveys. An index evaluating the spatial distribution and characteristics of the biomass on the ground would be helpful to monitor both the current state of different windthrow areas and their temporal changes. This index should also be appropriate to monitor felled forest in winter conditions (presence of snow cover) and the changing probability of avalanche release in relation to snow cover. Furthermore, the index should be computed using data available for large areas. Data derived from high-resolution LiDAR scans (Light Detection and Ranging) have become more frequent in the last decade, even for large areas (Niculiță, 2020). Different regions of the European Alps are already covered by LiDAR surveys since these are becoming more economically accessible to civil authorities (Doneus and Briese, 2011). The raw product of LiDAR surveys is a point cloud that is commonly processed to deduce digital elevation models (i.e., digital surface or terrain model). Forest elements such as trees, shrubs, lying stems and stumps could be identified and extracted for specific analysis (Burt et al., 2019; Dassot et al., 2011). For areas smaller than 10 ha, it is even possible to increase the digital surface model resolution up to a few centimeters by adopting the photogrammetric technique (analysis of pictures recorded with unmanned aerial systems, UAVs) (Colomina and Molina, 2014). In addition, the evaluation and the period of the minimum level of protective capacity provided by the biomass on the ground against snow avalanches are of high importance for the accurate management of these areas, including alternative scenarios. The achievement of such a result can be obtained through the analysis of windthrow areas for which data have been collected at different time steps since the disturbance.

Based on the state-of-the-art and gaps in knowledge, the objectives of this research are to (i) select and develop indices to assess the avalanche protective capacity of windthrow areas, (ii) assess the temporal change in protective capacity after a windthrow event, and (iii) evaluate the effect of the snow cover height on the increase in potential avalanche formation in windthrow areas. We investigated two study areas affected by windthrow to address these objectives. Temporal changes were observed in the long-term study area of Disentis, where high-resolution datasets at several timesteps were available (one survey was acquired approximately every ten years for a total of four datasets). The short-term changes and the influence of snow cover were assessed in the Franza study area using two high-resolution datasets that were capturing the summer conditions and one in the presence of snow cover. Using these datasets, we developed and tested two indices to evaluate the temporal changes and snow cover influence of protective capacity against snow avalanches.

2. Materials and methods

2.1. Study areas

Two study areas were selected to achieve the reported objectives: Disentis and Franza (Fig. 1). In the Disentis area (affected by the Vivian storm in 1990), we analyzed the characteristics of the biomass immediately after the storm event and in the following 29 years. At the Franza study site (impacted by the storm Vaia in 2018), we investigated the effect of snow cover smoothing relevant for possible avalanche formation and the short-term changes in biomass on the ground.

Within each study area, we manually defined the potential release areas (PRAs) of snow avalanches to spatially analyze their temporal evolution and the effect of snow cover on the protective capacity. To identify the PRAs, we used topographical variables such as slope, plan curvature, and presence of effective vegetation, using the thresholds from the literature. The slope angle was selected in the range of 28–55° (Bühler et al., 2013; Schweizer et al., 2003). We calculated plan curvature to separate concave from convex areas to identify ridges and then split or merge PRAs (Maggioni and Gruber, 2003). In addition, we considered effective vegetation to be 1.5 times higher than the maximum snow cover for a given return period (Saeki and Matsuoka, 1969). Furthermore, the relation between gap width and crown cover density was evaluated as a combination of crown coverage, gap length, and slope angle (Bebi et al., 2021; Frehner et al., 2005; Schneebeli and Bebi, 2004).

Every PRA was analyzed with indices assessing the vegetation height

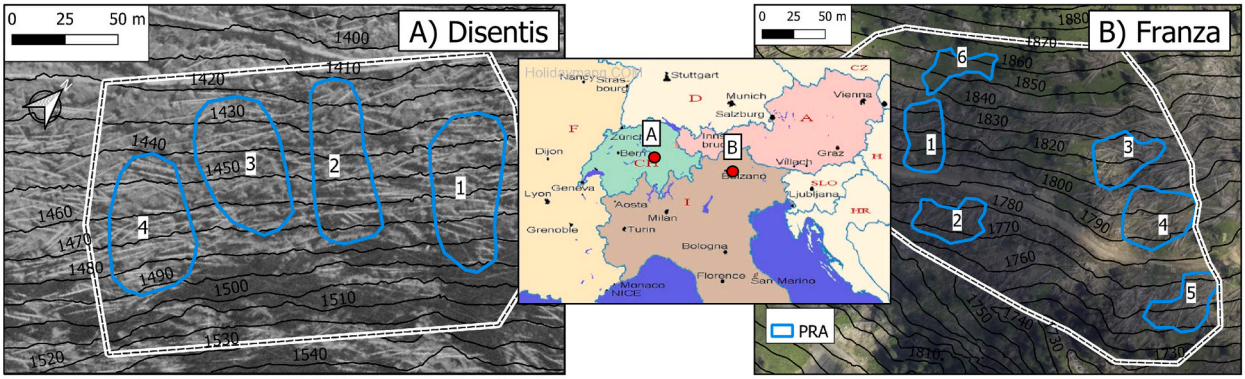

Fig. 1. Location and aerial images of the two study areas near Disentis (A) and Franza (B). The solid blue lines highlight the study sites. The identified potential release areas (PRAs) are outlined in blue. In the background, aerial orthophotos showing the postevent conditions, captured in 1990 and 2019 for Disentis and Franza, respectively. Please note the northing (A). (For interpretation of the references to colour in this figure legend, the reader is referred to the web version of this article.)

model (VHM), surface roughness, stored volume height and adapted tree parameters (see Section 2.2).

2.1.1. Disentis

The Disentis study area is located in the Swiss Alps, canton Grisons, and stretches over 2.14 ha. The elevation ranges between 1420 and 1560 m a.s.l., the aspect is northwest, and the slope is inclined between 30° and 50°. The site is in the low-subalpine zone of the Central Alps (Ellenberg and Leuschner, 2010), characterized by a mean annual temperature of 4 °C and mean annual precipitation of 1250 mm (Schönenberger et al., 2005). From a topographical point of view, the area is characterized by different zones of potential release or transit areas of snow avalanches. The Vivian storm occurred in February 1990, severely damaging the forest and affecting all the trees. Two-thirds of the trees were broken, one-third were uprooted (Schönenberger, 2002a, 2002b), and the site remained untouched to provide a monitoring research site (WSL). The prestorm stand was formed by a pure 110–150-year-old Norway spruce (*Picea abies*). Full callipering of the study area resulted in 363 stems ha^{-1} and 487 m^3ha^{-1} in 1972. We manually identified four potential release areas within the study site (Fig. 1A). The characteristics of the PRAs are reported in Table 2.

Site conditions were recorded by different photogrammetric surveys in 1991, 2001, 2009, and 2019. In 1991, 2001 and 2009, aerial photographs were taken by the Swiss Federal Office of Topography (swisstopo; colour, scale ~1:4′000). Analytical photogrammetry methods were performed by Frey and Thee (2002) and Bebi et al. (2015). The 2019 survey was recorded using a Mavic 2 Pro with ground control points (GCPs) acquired with a Stonex GNSS, and pictures were processed with Agisoft Metashape software (Agisoft LLC, St Petersburg, Russia). The derived dense point clouds and digital surface models (DSMs) were the input data for the following analyses (for specific information, see Table 1). The Digital Terrain Model (DTM) was acquired by a LiDAR survey in 2019 from the Swiss Federal Office of Topography with a resolution of 0.5 m (swisstopo).

2.1.2. Franza

The Franza study area is located in the Dolomites, Veneto Region, Italy (Fig. 1B). The elevation ranges between 1650 and 1950 m a.s.l. facing southwest. The site in the subalpine zone of the Eastern Alps is characterized by a mean annual temperature of 5 °C and a mean annual precipitation of 1100 mm (Barbi et al., 2013). The site covers 4.24 ha, and the slope inclination is between 25° and 40°. Storm Vaia severely hit the area in October 2018, destroying most of the forest stand (mainly by uprooting). The site was not involved in the forest management operations, but the roads were cleared of biomass. Approximately 5–10% of the original forest cover was not damaged. Meadows and young open forests cover the northern part of the area and are not affected by storms. The disturbed forest was dominated by Norway spruce (*P. abies*) with admixed silver fir (*Abies alba*) and European larch (*Larix decidua*), which was the only tree species resisting the storm. Within the study area, six PRAs were identified (Fig. 1B), of which five were covered by dense forest and one consisted of meadow (characteristics are reported in Table 2).

We captured the site conditions in 2019 and twice in 2020 with three drone flights. The derived dense point clouds and digital surface models (DSMs) served as input data for our following analyses (for specific information, see Table 1). Drone images were processed with the image processing software Agisoft Metashape (Agisoft LLC, St Petersburg, Russia). Ground control points were measured with a Topcon HiPer V GNSS, while images were acquired with a Dji Phantom 4 drone. The DTM was acquired by the Veneto Region in July 2019 with a LiDAR survey.

Table 1
Technical information of the photogrammetric surveys involving the Franza and Disentis study areas. The DTM (digital terrain model derived through LiDAR campaigns). GCP stands for the ground control point, DSM for the digital surface model and DTM for the digital terrain model.

Site	Date	GCP (n°)	GCP accuracy (x,y,z residual error, [m])	Point density [n° m^{-2}]	DSM resolution [m]	DTM (LiDAR) date, resolution [m]
Disentis (CH)	21/08/1991	*NA*	*NA*	22.5	0.20	2019, 0.50
	10/05/2001	*NA*	*NA*	22.5	0.20	2019, 0.50
	17/08/2009	*NA*	*NA*	22.5	0.20	2019, 0.50
	18/06/2019	10	0.147	680.2	0.10	2019, 0.50
Franza (IT)	26/10/2019	12	0.037	557.3	0.05	2019, 0.50
	29/10/2020	15	0.044	1500	0.05	2019, 0.50
	18/12/2020	11	0.103	1410	0.10	2019, 0.50

Table 2
Characteristics of the PRAs identified within the study areas.

Site	PRA	Area [m^2]	Slope angle [°]	Aspect [°]	Prestorm crown cover density [m^2/m^2]	Post-storm crown cover density [m^2/m^2]
Disentis (CH)	1	*1852*	*41*	141	1.00	0.02
	2	*2886*	*37*	135	1.00	0.05
	3	*3090*	*38*	136	1.00	0.02
	4	1133	40	142	1.00	0.01
Franza (IT)	1	1131	31	187	0.85	0.00
	2	1055	34	188	1.00	0.01
	3	1159	41	180	1.00	0.02
	4	1593	32	168	1.00	0.00
	5	1146	32	175	0.92	0.02
	6	710	36	192	0.00	0.00

The cloud point density and digital terrain resolution values reported in Table 1 represent the quality of the original data. In this study, we reduced these values to compare the index results of the different surveys in terms of time variations and study areas. The data quality adopted for the different indices is reported in the relative description.

2.2. Indices

We analyzed the identified potential release areas with four different indices to assess the forest protective capacity over time and evaluate the snow cover effect. Vegetation height models (*VHM*) and surface roughness models (*SR*) are common indices used to study the height of biomass concerning ground and surface variability within a specific moving window (Grohmann et al., 2011). To improve the characterization of windthrow areas, we developed the stored volume height (*SVH*) index and the adapted tree parameters (*ATP*). We used the reported datasets to test the efficiency of the proposed indices and, at the same time, investigate the temporal evolution of windthrow areas and the effect of snow cover.

2.2.1. Vegetation height model (VHM)

The *vegetation height model* (*VHM*) was calculated as the difference between DSM and DTM. For each area, we used the same DTM (derived from the LiDAR survey) since no topographical changes, such as mass movements, were observed within the identified PRAs. To calculate the *VHM* for every survey, we used DSMs derived from each photogrammetric survey to capture the changing surface. The resolution of the DTM and of the most recent DSM of the Disentis study area reported in Table 1 were interpolated to 0.20 m to match the DSM resolution of the first three surveys by adopting a bicubic method (Brovelli et al., 2004). We then extracted the cell values within every identified PRA, to accurately analyze the developments in vegetation height. We performed the *VHM* analysis for the Disentis study area only because of the availability of a long time series (29 years). Identification of the vegetation height was not possible using the photogrammetric technique in winter conditions, so it was not performed at the Franza site.

2.2.2. Surface roughness (SR)

We further tested the performance of the *surface roughness* (*SR*) to detect the change in windthrow areas over time and with the presence of snow cover. We used the vector ruggedness measure (Sappington et al., 2007) algorithm to compute *surface roughness*. The input data were the photogrammetric-derived DSM. The resolution and moving window size were 1 m and 7 × 7, respectively (Brožová et al., 2021). We resampled the DSM with a mean value method to obtain the desired resolution of 1 m. The resulting raster map was analyzed, extracting the cell values within the identified PRAs.

2.2.3. Stored volume height (SVH)

The *stored volume height* index (*SVH*) was based on the calculation of the volume between two layers. We used the high-resolution DSM as the first layer, and the second layer was derived using the highest point of the original DSM to smooth the original surface. The final map conceptually represents a good proxy for the necessary volume of snow required to fill the rough surface (resulting from the felled trees) to obtain an entirely smooth surface. We derived the volume for a given PRA and calculated a normalized height (*SVH*) by dividing the volume by the area.

We report the algorithm to compute *SVH* in a flowchart (Fig. 2). We used the functions implemented in the "lidR" package (Roussel et al., 2020) to analyze and process point clouds in R (R Core Team, 2021). First, the outliers were removed using the Statistical Outliers Algorithm SOR (Rusu and Cousins, 2011), with the number of neighbors equal to 8 and multiplier equal to 3. Next, we classified the dense cloud (photogrammetrically derived) into two classes: high vegetation (represented by trees and their crowns) and the rest (product 1 in Fig. 2). We used the Cloth Simulation Filtering algorithm (Zhang et al., 2016) to separate the two classes using a cloth resolution of 0.5 m, a classification threshold of 3.0 m and activating the steep slope function. We removed the points from the point cloud classified as high vegetation and calculated a DSM with a cell resolution of 0.5 m taking the maximum elevation value within the grid cell (product 2 in Fig. 2). The algorithm then computed the difference between the DSM and DTM, obtaining the low vegetation height model (LVHM, product 3). From this layer, we calculated a smooth surface (product 5 in Fig. 2), first resampling the LVHM to a resolution of 2.5 m (method: highest value, product 4) and then interpolating it to the original resolution of 0.5 m (method: bilinear). Finally, we computed the smooth difference as the difference between the

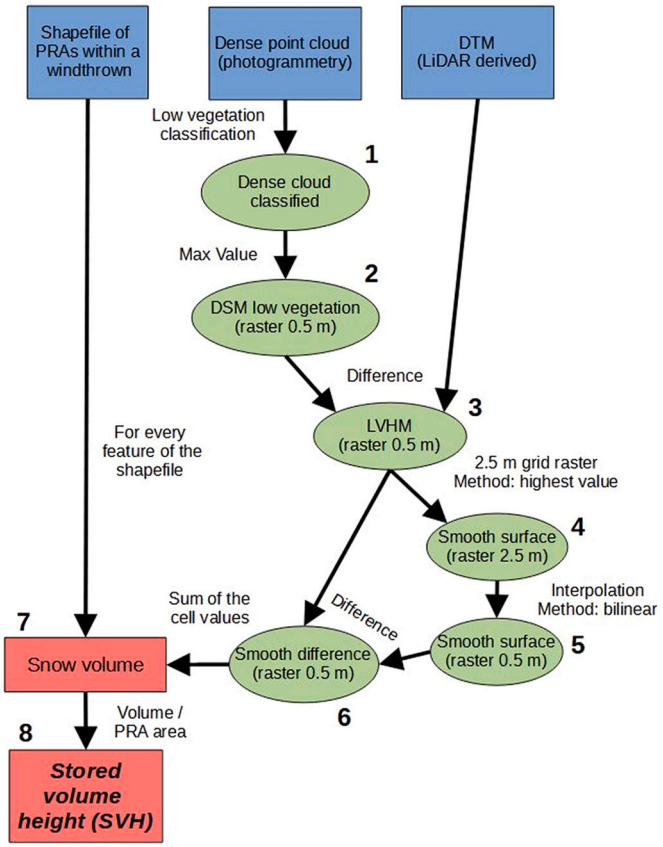

Fig. 2. Flowchart of the stored volume height algorithm: blue polygons represent input data; the raster or point cloud data are in green; numeric values are in red. DTM stands for digital terrain model. (For interpretation of the references to colour in this figure legend, the reader is referred to the web version of this article.)

smooth surface and the LVHM (product 6). Summing up the values of the smooth difference layer within a PRA, we calculated the volume necessary to smooth the original surface (product 7 in Fig. 2). Then, by dividing the volume for the PRA extension, we calculated the *SVH*. The *SVH* can be considered the mean value of snow height necessary to fill the irregular surface of a given PRA. The presented algorithm was implemented in R language (Baggio, 2021) and is freely available.

The algorithm removed points representing high vegetation to avoid extreme values of the smoothed difference surrounding standing trees. If the points had not been removed, the *SV* for a given PRA would result in an excessive value. The *stored volume height* approach was designed to assess the irregularity of the biomass felled by the storm, not including higher vegetation. To compare the results of the different surveys for the two study areas, the original dense clouds (Table 1) were decimated with a random function to the point density of the survey characterized by the lowest resolution (22.5 points/m^2).

2.2.4. Adapted tree parameters (ATP)

For the identified PRAs at the Disentis site, we analyzed the forest parameters of tree density and crown cover. The tree and crown identification algorithm was implemented in R (R Core Team, 2021) using the functions of the "lidR" package (Roussel et al., 2020). The input data were the dense point cloud and LiDAR-derived DTM. We first removed the outlier points with the SOR function (Rusu and Cousins, 2011) and then normalized the point cloud with the DTM. We identified the treetops using the *lmf* algorithm (Popescu and Wynne, 2004) based on a local maximum filter. We applied a circular fixed moving window of 7 × 7 m, and the height threshold for tree segmentation equaled 1.5 times the maximum snow depth (the calculated 30-year return period maximum snow depth in Disentis was 2.50 m) (Frey and Thee, 2002). We identified the crown area based on the Silva et al. (2016) algorithm, adopting default parameters. In such a way, the identified tree height was referred to as the ground level. In the case of windthrow areas, we assumed that snow accumulates on the fallen biomass layer and not directly on the ground. Therefore, the height of a standing tree should be referred to the height of the biomass on the ground. For this reason, we delineated a circular buffer area around every identified tree crown of 4 m. We calculated the mean height with respect to the ground for each of these buffer areas (equal to the biomass height above the ground, $H_{ground\ biomass}$, Fig. 3B). The corrected tree height ($H_{tree\ corrected}$) was the difference between the original height with respect to ground level (H_{tree}) and the mean height of the fallen biomass surrounding the tree ($H_{ground\ biomass}$), as shown in Fig. 3B. Finally, we considered the tree presence within a given PRA if $H_{tree\ corrected}$ resulted greater than 1.5 times the maximum snow depth in a return period of 30 years. Dividing the number of trees and total crown area by the relative PRA extent, we obtained the tree density and cover percentage, respectively. The algorithm to derive the reported *adapted tree parameters* from a point cloud was implemented in R language (Baggio, 2021) and is freely available. As described for the *SVH* index, the original point clouds were decimated with a random function to match the point density of the survey with the lowest point resolution, equal to 22.5 points/m^2.

Furthermore, we assessed the presence of critical gaps within the forest cover as a potential cause of snow avalanche release areas. The gap length was evaluated within the identified PRAs along the maximum slope. We adopted the thresholds reported in Schneebeli and Bebi (2004) for critical gap identification (Fig. 3A). The delineation was based on a function between gap length and crown cover density for different classes of slope steepness.

2.3. Additional analysis

To accurately assess the performance of the *SVH* index and the variation in biomass height, we computed the DEM of Difference (DoD) for the Franza study area. DoD is the difference between the two elevation models, and in this case, we used two DSM maps without snow cover. To accurately compute the DoD map, we adopted the minimum level of detection method (Brasington et al., 2003) estimated as the DoD error. The DoD error results from Eq. 1, where δu_1 and δu_2 are the errors of the photogrammetric derived surveys. The errors associated with every survey are reported in Table 1.

$$\delta u_{DoD} = \sqrt{\delta u_1^2 + \delta u_2^2} \quad (1)$$

During the photogrammetric survey of the Franza area on 18 December 2020, we measured the height of the snow cover. The height was measured perpendicular to the surface using a ruler. We collected six measurements in separate locations of the study area, characterized by the absence of felled trees. We surveyed five values for every measurement: four at the vertices of an imaginary square with 1 m sides and one in the middle. The five values were averaged to derive a single measurement for the given location.

To estimate the necessary amount of snow to smooth the irregular surface created by the biomass on the ground, we fitted a linear model between snow depth and the values of *SVH* observed in October 2020 and December 2020 for the Franza study area. The objective of the

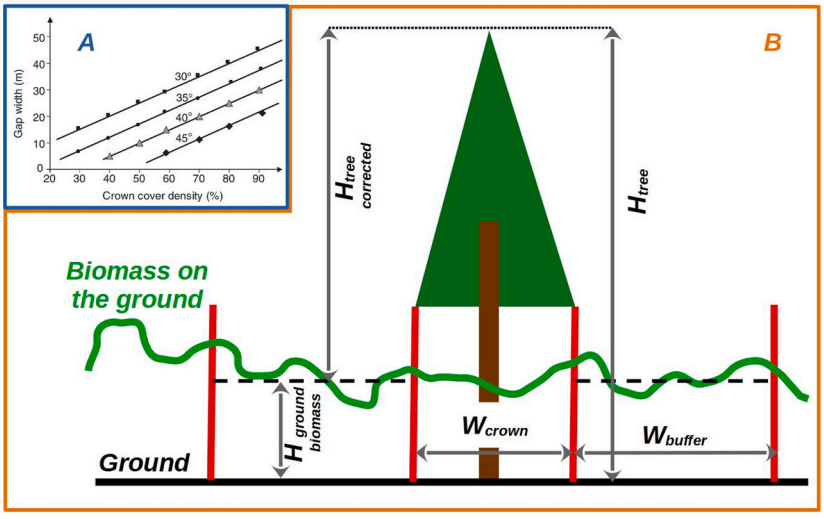

Fig. 3. A) Relations between gap width and crown cover density for critical gap identification (source: Schneebeli and Bebi, 2004). B) Sketch of a standing tree in a windthrow area with the reported measures used to improve the calculation of tree height in accordance with the biomass on the ground.

analysis was to extrapolate a threshold in snow depth for which the *SVH* values observed in October 2020 for PRA 1–5 (windthrow areas) decreased toward the *SVH* of PRA 6 (meadow area, Fig. 1B).

3. Results

3.1. Temporal change: Disentis

We observed a temporal change in forest protective capacity over 29 years at the Disentis site by using all four indices: *vegetation height model (VHM)*, *surface roughness (SR)*, *stored volume height (SVH)* and *adapted tree parameters (ATP)*. Similar trends were noticed when using the three indices (*VHM*, *SR* and *SVH*), with an observed minimum in 2001 (Fig. 4). However, the *adapted tree parameter* index showed a minimum one year after the disturbance in 1991 (Fig. 4 and Fig. 5). According to the *ATP,* there were almost no trees one year after the disturbance (Table 3). Furthermore, it is important to observe the variability between the identified PRAs in 1991 for the three indices reported in Fig. 4. The mean *VHM* ranged between 1.41 and 2.50 m, the mean *SR ranged* between 0.116 and 0.198 and the *SVH* index ranged between 0.735 and 0.973 m.

Nineteen years after the storm event, all the indices (*VHM*, *SR*, *SVH* and *ATP*) showed an increase with greater values compared to the first survey (immediately after the disturbance). In 2009, there were some trees up to 14 m in height. However, variability between different PRAs was observed, and PRA 3 had only a few trees (Fig. 5 and Table 3).

For the fourth survey (in 2019), *surface roughness* and *stored volume height* slightly increased compared to the previous years. The only exception involved the *surface roughness* of PRA 1, which showed a decreasing trend over the last nine years. The *stored volume height* values were similar between the four PRAs, while the *surface roughness* values showed a higher variability. Instead, the *VHM* showed a constantly increasing trend since the minimum observed in 2001. However, the increase in *VHM* values at PRA 3 was lower than that of the other PRAs. Similarly, the *ATP* index showed an increasing number of trees with some variability per PRA, with the fewest trees in PRA 2 (Fig. 5 and Table 3).

Regarding the *adapted tree parameters*, the analysis showed 1 to 3 standing trees per PRA immediately after the storm (in 1991), while crown cover density was between 1.6 and 5.1%. The trends of the number of trees and crown cover increased over time for all the PRAs. Instead, PRA 1 and 2 showed a slight decreasing trend of tree density

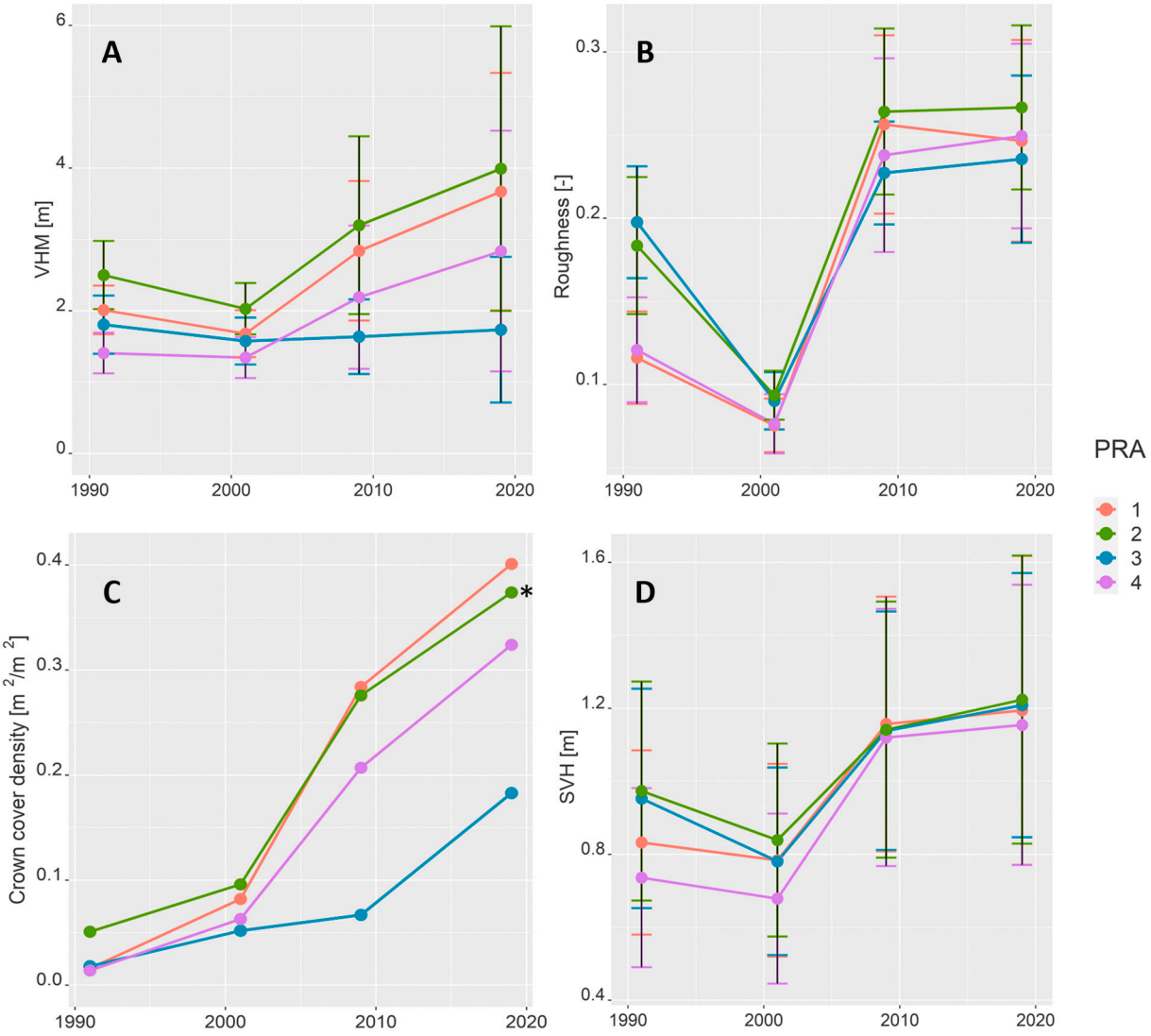

Fig. 4. Plots showing the mean value of the four investigated indices for every PRA and photogrammetric survey of the Disentis study site: (A) vegetation height model (VHM), (B) surface roughness, (C) crown cover density, and (D) stored volume height. The locations of the PRAs are reported in Fig. 1. The symbol * in the (C) plot indicates the absence of critical gaps, as defined in Schneebeli and Bebi (2004).

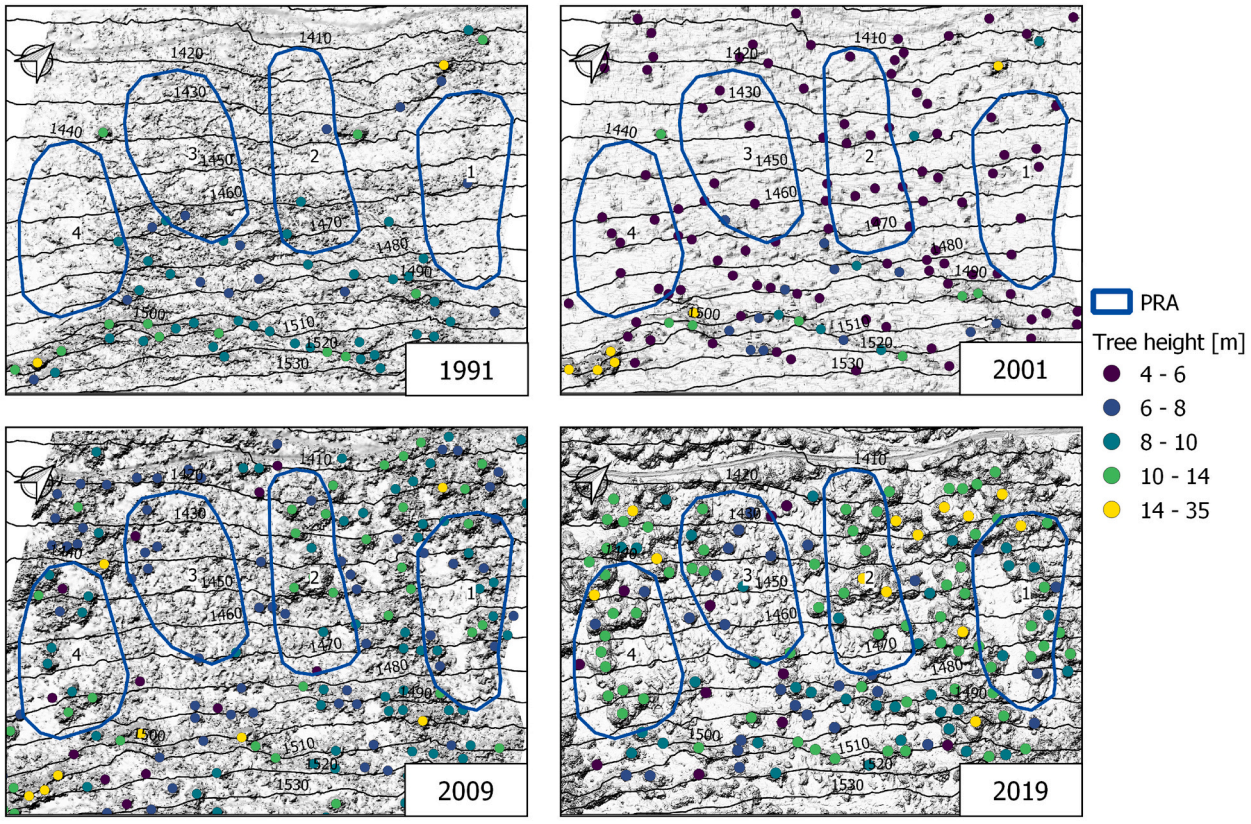

Fig. 5. Maps of the calculated tree positions at the Disentis study site based on the algorithm "adapted tree parameters" described in Section 2.2.4 for the years 1991, 2001, 2009, and 2019. The different colored dots represent the tree height [m] with respect to the ground level. In the background, we plotted the hillshade view of the DSM photogrammetry-derived survey. The elevation difference between contour lines is 10 m. The solid blue lines depict the PRAs. (For interpretation of the references to colour in this figure legend, the reader is referred to the web version of this article.)

Table 3
Tree density of the potential release areas PRAs (Fig. 5) per date of photogrammetric survey of the Disentis study area.

Tree density [n°/ha]				
PRA	1991	2001	2009	2019
1	4.8	38.3	76.6	71.8
2	15.5	51.6	56.8	51.6
3	4.6	27.5	32.1	64.1
4	4.7	37.7	51.8	70.7

between 2009 and 2019 (Table 3). The major increment of tree density occurred between 1991 and 2001 (Table 3) and for the crown cover density between 2001 and 2009 (Fig. 4 C). In 2019 (29 years after the storm), the mean tree density of the four PRAs was 64.5 trees ha^{-1}, and the crown cover density was 33.4%. These values vary between 20.1 trees ha^{-1} and 20.7% regarding the tree and crown cover densities, respectively. Twenty-nine years after the storm, we identified the presence of critical gaps (Section 2.2.4) in three PRAs (PRA 1, 3 and 4), which might be prone to avalanche formation. Only PRA 2 showed a full recovery without critical gaps in 2019 (Fig. 4). The identified PRAs showed different recovery patterns in forest protective capacity even if the preevent conditions were similar.

3.2. Short-term change and snow cover effect: Franza

At the Franza study area, the values for *surface roughness* and *stored volume height* differed depending on the date of the data acquisition (Fig. 6). The difference between October 2019 and October 2020 (both surveys without snow cover) showed a decreasing trend in *surface roughness*. In contrast, the *stored volume height* showed an increase between the same dates, except for PRA 2 (Fig. 6 B).

From the DoD map of PRA 3 (Fig. 7), it was possible to visually determine that most of the stems did not move during the 2019/2020 winter season (difference between the DSM acquired in October 2019 and October 2020). However, needles and small branches broke down, reducing the elevation values identifiable from the crowns of felled trees (Fig. 7). This process resulted in new spaces between logs that slightly increased the amount of snow required to smooth the irregular surface. This process was captured by the *SVH* (increasing trend), while the *SR* did not capture the change in stem structure (decreasing trend, Fig. 6A).

The *SVH* and *SR*, calculated in December 2020 with snow cover, were lower than those of the previous survey without snow cover (October 2021). The snow depth measured the same day as the photogrammetric survey was 0.85 m (mean of six measurements taken in different locations of the study area). Considering the snow cover, the *stored volume height* of PRA 1–5 surveyed in December 2020 (mean value of 0.67 m) was higher than the grassland control area of PRA 6 (equal to 0.15 m). The mean percentage decrease in stored volume in the PRAs (excluding PRA 6) was 18% (with a range of 14–25%). Hypothesizing a decreasing linear trend of the *SVH* index as a function of snow depth, we derived a linear model using the *SVH* values recorded in October 2020 and December 2019 for PRA 1–5, obtaining a coefficient of −0.18 per meter of snow. Adopting the fitted model to estimate the snow height necessary to decrease the *SVH* of PRA 1–5 toward the mean *SVH* value of PRA 6 (recorded in October 2020), we calculated a value of 3.35 m. This value may represent the snow depth necessary to smooth the rough surface generated by the biomass on the ground for which snow avalanches may be released.

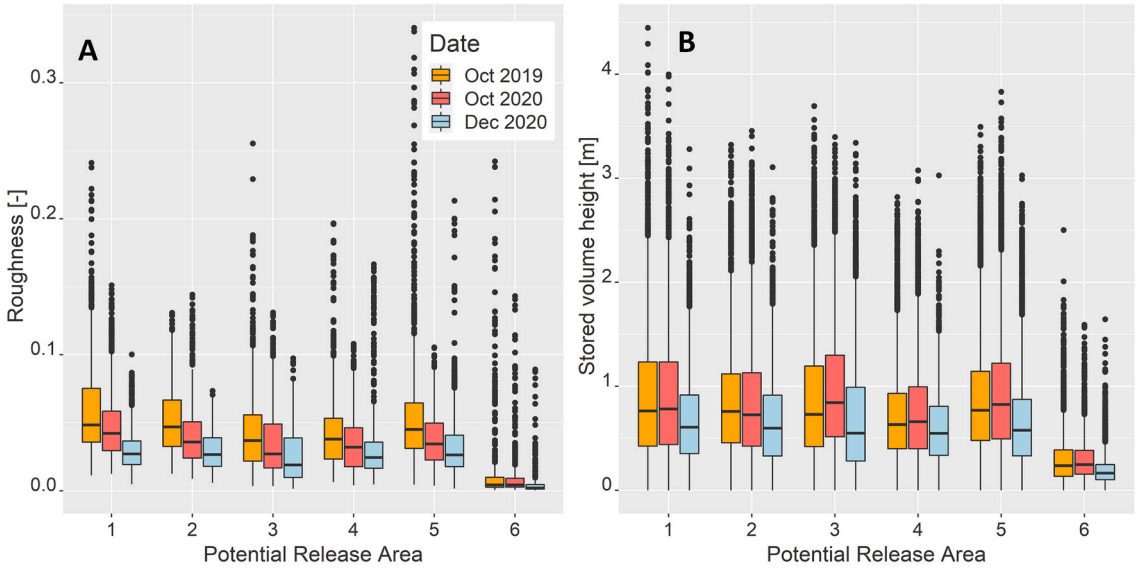

Fig. 6. Raster point analysis of potential release areas (PRAs) of the Franza site for surface roughness (SR) (A) and stored volume height (SVH) (B). The black line within the boxplot represents the mean value, and the boxplot upper and lower limits are the 25th and 75th percentiles.

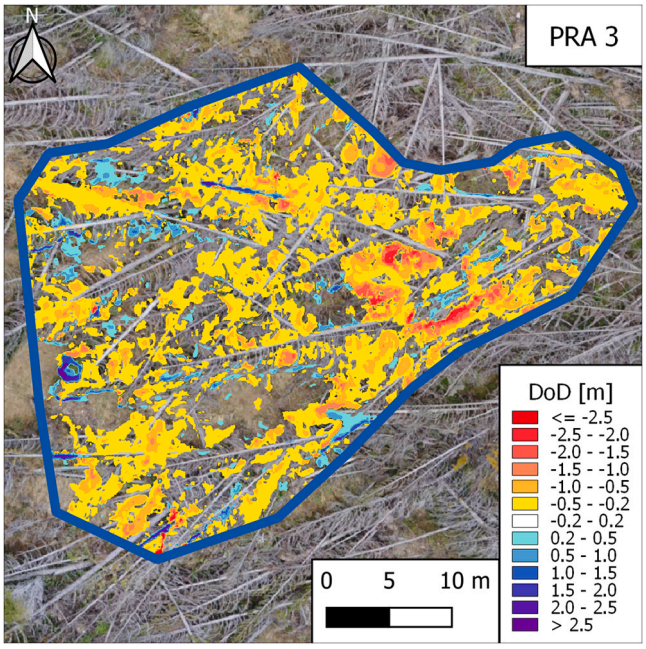

Fig. 7. Digital elevation model of Difference (DoD) map of the potential release area 3 (PRA 3) within the Franza study area. The PRA location is shown in Fig. 1B.

4. Discussion

4.1. Temporal change: Disentis

The results of the indices in the Disentis study area (Fig. 4) were consistent in assessing the minimum level of forest protective capacity in 2001, 11 years after the storm event. The *SVH* index showed a decreasing trend between 1991 and 2001, highlighting the reduction in space between the felled trees and thus decreasing the protective capacity of the plots in mitigating the release of snow avalanches. Nineteen years after the storm (in 2009), the protective capacity was higher than one year and 10 years after the event. The *SVH* and *ATP* values showed an increasing trend between the surveys recorded in 2001, 2009 and 2019 (Fig. 4). The increase in forest protection identified by the adopted indices for the 2009 and 2019 surveys was mainly due to the growth of shrubs and young trees, which started to increase the protective capacity against the potential release of snow avalanches (Brožová et al., 2020; Germain et al., 2005; McClung, 2001; Viglietti et al., 2010). Regarding the growing forest, the tree and crown cover density are crucial indices for assessing forest protection and identifying gaps (Frehner et al., 2005; Schneebeli and Bebi, 2004; Swanson and Stevenson, 1979). Therefore, the trees were identified only if their height exceeds a threshold value with respect to the surrounding surface (Fig. 3B). Analyzing values of the *adapted tree parameter* (Fig. 5), we found one PRA (from the total of four), showing no critical gaps 29 years after the disturbance according to the thresholds reported by Frehner et al. (2005). Looking at the tree density and crown cover density between 1991 and 2001, it was possible to identify a positive trend. It is likely that predisturbance regeneration took advantage of light availability after the trees were felled by the storm. Between 2001 and 2009, we observed a continuously increasing amount of vegetation, and the canopy cover density reached values up to 0.27. For the following survey (in 2019), the trend slightly decreased in intensity, but the indices reached values of 0.20–0.40 in crown cover density. Looking at the values of *SVH* and *ATP*, it was possible to estimate the minimum level of protection occurring 10 years after the storm event, i.e., in 2001. The extent of the original PRAs was reduced by the forest cover 19 years after the storm and further in the following 10 years. Consequently, the extent of PRAs and the related avalanche volume decreased with time after disturbance. Accordingly, Teich et al. (2014) highlighted the increase in small snow avalanches stopping within sparse/young forests. Furthermore, even slow forest recovery contributed to forest protective capacity in stabilizing the snowpack to some extent. In general, a few small gaps could be found between young trees, which might be prone to avalanche formation. The identification and evaluation of such small gaps and forest parameters are of great interest to reliably simulate possible snow avalanches (Brožová et al., 2020). Evaluation of the low vegetation merits particular attention, which does not always provide adequate protection on steep slopes, as it might be compressed by snow cover (Feistl et al., 2014). However, small avalanches may be triggered within the identified plots under particular meteorological conditions, i.e., snowfall occurrence in the late winter season associated with high temperatures. Such avalanches can probably be stopped by the forest, but they could break young trees,

damaging the natural regeneration and delaying the establishment of an effective protection forest. Nevertheless, no avalanches were observed in the uncleared windthrow study area of Disentis (Wohlgemuth et al., 2017). The most intense winter in terms of cumulative snow cover depth was 1998/1999, with a maximum value of 1.65 m (Frey and Thee, 2002). This value was lower than the expected height with a return period of 10 years (calculated in accordance with Buwal (1990) for the Disentis study area). However, even if around the moment of lower values in terms of *SVH* (Fig. 4), the felled trees probably stabilized the snow cover, preventing the release of snow avalanches during the winter season. Instead, snow avalanches were observed particularly after an intense snowfall event (occurring on 16/04/1999 with a total snowfall amount of approximately 1 m) in areas adjacent to the one studied by Frey and Thee (2002). This observation can support the protective capacity of felled trees, but it is important to accurately evaluate the amount of snow on the ground and the timing and frequency of snowfall during the winter season (Schaerer, 1977).

4.2. Short-term change and snow cover effect: Franza

The DoD map (Fig. 7) showing the surface elevational changes in one year (comparison between the summer surveys of 2019 and 2020) highlighted that most of the fine biomass (needles and small branches) fell on the ground or broke (Radtke et al., 2009). This process left more space to store the snow between the lying stems and consequently increased the snowpack stability. In this case, the protective capacity against snow avalanches slightly increased two years after the windstorm compared to one year after. However, such a minor increase in protective capacity was expected to rapidly decrease within the next ten years, as observed in the Disentis study area. Regarding the influence of snow on terrain smoothing, promising results were obtained by investigating the *stored volume height* with and without snow cover. The index decreased for every PRA compared to the absence of snow. However, the *SVH* values of PRA affected by windthrow were noticeably higher than a smooth PRA, meaning that more snow could be accumulated without the risk of releasing an avalanche (for the December 2020 survey of the Franza site). After the storm event at Franza, the abated protection forest showed a good function in storing and supporting snow cover, considering the snow depth and *stored volume height* values observed in winter conditions. The protection is also expected to be sufficient with a snow depth greater than that of the December 2020 survey (0.85 m measured in the meadow next to the forest). The extrapolation of the fitted linear model calculated a snow depth value of 3.35 m necessary to smooth the observed surface of windthrow areas toward the same level as meadow areas. This value of snow depth is expected to decrease over the years due to *SVH* decrease, as observed in the Disentis area, where the minimum was observed ten years after the storm event. However, the estimation is approximate since the model is based on only one survey representing winter conditions. Additional validations are necessary to correctly establish a robust relationship between snow depth and *stored volume height* to improve the predictability for the potential formation of snow avalanches depending on the snow depth.

4.3. Applications and limitations

The protective capacity of forests affected by windthrow disturbance in terms of temporal development and snow cover influence was assessed using four indices. The *stored volume height* index, representing the snow volume needed to fill the space to create a smooth surface, was suitable to investigate both the temporal change and the effect of snow cover in areas affected by wind disturbance. The index performed a direct spatial estimation of the volume left by trees and crowns on the ground, examining the difference between the original DSM and a smoothed DSM. Moreover, *SVH* did not consider trees above a certain height to avoid deviating the estimation of the dominant fallen biomass. The index *stored volume height* was more suitable than *surface roughness* for the estimation of forest protection against snow avalanches after a disturbance. This finding is supported by the results from the Franza study area, where the breakage process increased the free volume between the tree stems (Fig. 7). The *stored volume height* captured this aspect, as observed by the increasing trend between the surveys of October 2019 and October 2020 (Fig. 6 B).

We further developed an automatic procedure to identify standing trees and extract the related crown area and tree density. The procedure identifies trees emerging from a certain threshold above the mean height of the biomass surrounding the target tree. Due to the availability of LiDAR data, different algorithms have been developed in recent years to automatically identify and segment trees (Burt et al., 2019; Popescu and Wynne, 2004). The common reference surface for tree height estimation is the ground, usually derived from the last return of the laser signal (Mkaouar et al., 2018). This approach is appropriate for biomass estimation or growth rate calculation (Qi et al., 2019; Zhao et al., 2018). In contrast, the reference surface for snow avalanches should be at the point of avalanche formation. In the case of windthrow areas, the reference surface is expected to be above the biomass layer deposited on the ground, where weak layers may develop (Schweizer et al., 2003). Meyer-Grass (1987) observed that the protective function of forests is predominantly correlated with stem density. This finding is supported by the study of Viglietti et al. (2010), for which a dataset of snow avalanches triggered within forests of the Valle d'Aosta region (Italy) was analyzed. Perzl (2005) reported that a crown cover density of 50–60% can be a threshold value to define the protection forest in situations with a relatively low terrain roughness. The study confirms that lower threshold values of crown cover may be adequate in the case of disturbed areas characterized by high terrain roughness. McClung (2001) observed the release of a few avalanches in areas where the vegetation height was higher than 4 m. In Germain et al. (2005), the avalanche activity observed in postlogging and postfire locations was stopped by postdisturbance natural regeneration. In particular, the postfire period for which avalanches can occur was assessed to be 15–20 years. In this sense, the proposed *ATP* index (Fig. 3) satisfactorily identified trees emerging from the reference surface for snow avalanches formation considering only the trees that potentially provide effective protection. Practitioners can adopt the index to classify the protective capacity of distinct types of forests.

The investigated study areas highlighted the importance of using spatial indices to assess the protective capacity of windthrow areas concerning snow avalanches. Given the relatively low intrasite variability in pre-storm forest characteristics and topographical conditions, differences in terms of deadwood decay and natural regeneration were detected between the PRAs at both sites. In Disentis, the differences were related to the natural regeneration of trees (index: *adapted tree parameters*) and the decay of deadwood (index: *stored volume height*). One particular PRA showed forest cover with no critical gaps 29 years after the event, while for other PRAs, the tree growth rate was lower, and critical gaps existed. Even if some areas present small gaps, the likelihood of triggering snow avalanches is expected to be low due to the rough surface generated by shrubs and young trees. This example of site variability shows the need for an accurate evaluation of the postdisturbance forest protective capacity. For this purpose, the study reports a new spatially distributed index to evaluate the residual protective capacity of forests (*SVH*) affected by storms together with an algorithm to automatically identify the presence of remaining or new trees (and the related crown extent) emerging from the biomass on the ground (*ATP*). The combination of *SVH* and *ATP* improves the knowledge of the dynamics in windthrow areas supporting and integrating previous studies (Bebi et al., 2015; Frey and Thee, 2002; Schönenberger et al., 2005; Wohlgemuth et al., 2017). The indices can potentially be used over large regions covered by LiDAR or photogrammetric surveys (Bühler et al., 2022). Practitioners and civil authorities can benefit from such tools, and they can quickly identify high-risk areas to develop warning systems in accordance with the height of the snow cover and

the characteristics of the biomass on the ground. In the long term, the indices have the potential to map areas with lower protective capacity supporting decision-making on the establishment of necessary technical countermeasures.

To adequately assess and improve the quality and accuracy of the indices, further studies and control areas are desirable, especially considering different forest characteristics such as density, age structure, species composition and disturbance intensity. In particular, field surveys involving the exact quantification and displacement of the biomass on the ground are desirable to confirm and improve the outcomes of the indices. Additionally, a large number of winter photogrammetric surveys are needed to better assess the relationship between snow height and the effect of surface roughness smoothing. These kinds of surveys would be beneficial, but at the same time, they are difficult to collect. The potential accessibility in windthrow areas is laborious, and the increase in snow cover can lead to an increase in avalanche danger with higher risk.

The methods reported in this study may also be used to assess protective capacity against rockfall of windthrow forests. Felled trees have a great capacity to influence rockfall runout distance (Olmedo et al., 2015). Lying stems increase the surface, consequently increasing the probability of impacting obstacles and decreasing the associated energy (Ringenbach et al., 2021). Moreover, the tree identification algorithm can be used to delineate the characteristics and location of new forested areas. Such data serve as a fundamental input to update rockfall hazard maps in areas impacted by storms in the past, since disturbed forests have great importance in rockfall hazard mitigation (Lingua et al., 2020; Scheidl et al., 2020). Regarding forests affected by bark beetle outbreaks, Teich et al. (2019) observed a more heterogeneous snow stratigraphy compared to areas where salvage logging operations took place. Heterogeneity further increased in accordance with the remaining canopy cover. In the end, it is suggested to leave dead trees in place, particularly where the population reached epidemic characteristics (Caduff et al., 2022). For forests disturbed by bark beetles, which are further expected to increase in the future as a consequence of climate change (Bentz et al., 2010), the ATP index can be used to monitor the remaining crown cover and *SVH* to assess the characteristics of the biomass on the ground.

Assessing post-disturbance forest effects against natural hazards is crucial (Bebi et al., 2017). The evaluation of hazard protection in disturbed areas could become difficult due to their extension and problematic accessibility, as observed in areas affected by disturbances in the alpine region (e.g., large forested areas disturbed by the Vaia storm in 2018). This study introduces innovative methods to assess and monitor the temporal evolution of forest protective capacity affected by a disturbance event. Such methods can be directly applied to evaluate the post-disturbance forest protective capacity even in large areas, since the required input data are point clouds derived from LiDAR or photogrammetric surveys. Consequently, civil authorities could quickly define post-disturbance forest protective capacity over large areas, identifying sites with lower protective capacity requiring immediate management. The described methods can be further used to compute different management scenarios in a spatial-temporal framework to derive the most promising option. The analysis can be used to investigate the consequences of recent disturbances (storm Vaia 2018, Chirici et al., 2019) and monitor the temporal evolution of past disturbances (Quine and Bell, 1998) for immediate management of hazard areas.

5. Conclusions

This study investigated the protective capacity of windthrow forests thanks to two study areas in the European Alps (Disentis, Switzerland and Franza, Italy) that were recorded by high-resolution photogrammetric surveys. Thanks to multitemporal surveys, the minimum level of protective capacity was assessed approximately ten years after the disturbance when the protective effect of the biomass on the ground was at a minimum, and natural regeneration was not yet sufficiently developed. Twenty-nine years after the disturbance, the trees reduced the PRA area extent and fragmented the original PRA, decreasing the potential size and effects of possible snow avalanches. Among the four indices considered in this study, the *stored volume height* and the *adapted tree parameters* were the best indices to assess and monitor the protective capacity of forests affected by windstorms. In particular, the *stored volume height* performed well in characterizing the effect of snow cover on the biomass on the ground. The combination of *stored volume height* and *adapted tree parameters* allows the analysis of the characteristics of the biomass on the ground, the remaining standing trees and the development of natural regeneration. The indices presented in this study can be used at a regional scale to spatially assess and monitor forest conditions affected by windthrow, improving the management of the most critical areas over time.

Research data

The codes to compute the stored volume height and the adapted tree are available at the following link: https://github.com/TommBagg/Wind-disturbed_forest_analysis/releases/tag/WDFA_v1.0 (last access 12 December 2021), doi:https://doi.org/10.5281/zenodo.5771996, Baggio, 2021.

Data are available from the corresponding author upon request.

Credit author statement

Tommaso Baggio conceptualised the research, developed the scripts, collected field data, performed the analysis and wrote the manuscript. Natalie Brožová and Alexander Bast collected field data and reviewed the manuscript. Peter Bebi provided historical data and reviewed the manuscript. Vincenzo D'Agostino improved the research structure and reviewed the manuscript.

Declaration of Competing Interest

The authors declare that they have no known competing financial interests or personal relationships that could have appeared to influence the work reported in this paper.

Acknowledgments

This research received funding as part of the project "Bridging the mass-flow modeling with the reality", from the CARIPARO foundation [2724/2018]. The research was also supported by Dept. TESAF in the frame of the project Vaia-FRONT (BIRD-UniPD 2019-2021). This work was partly funded by the WSL research program Climate Change Impacts on Alpine Mass Movements – CCAMM (ccamm.slf.ch). The authors wish to thank Lorenzo Martini (TESAF Department) for performing the three drone flight surveys of the Franza study area. We are grateful to the three anonymous reviewers for their useful suggestions.

References

Allan, R.P., Hawkins, E., Bellouin, N., Collins, B., 2021. IPCC, 2021: Summary for Policymakers. IPCC.

Baggio, T., 2021. Wind-disturbed_forest_analysis_v1.0 [code]. https://doi.org/10.5281/zenodo.5771996.

Barbi, A., Checchetto, F., Delillo, I., Rech, F., 2013. Le precipitazioni sul Veneto-Valori annuali.

Bebi, P., Putallaz, J.M., Fankhauser, M., Schmid, U., Schwitter, R., Gerber, W., 2015. Die Schutzfunktion in Windwurfflächen. Schweizerische Zeitschrift fur Forstwes. 166, 168–176. https://doi.org/10.3188/szf.2015.0168.

Bebi, P., Seidl, R., Motta, R., Fuhr, M., Firm, D., Krumm, F., Conedera, M., Ginzler, C., Wohlgemuth, T., Kulakowski, D., 2017. Changes of forest cover and disturbance regimes in the mountain forests of the Alps. For. Ecol. Manag. 388, 43–56. https://doi.org/10.1016/j.foreco.2016.10.028.

Bebi, P., Bast, A., Ginzler, C., Rickli, C., Schöngrundner, K., Graf, F., 2019. Waldentwicklung und flachgründige Rutschungen: eine grossflächige GIS-Analyse.

Schweizerische Zeitschrift fur Forstwes 170, 318–325. https://doi.org/10.3188/szf.2019.0318.
Bebi, P., Bast, A., Helzel, K., Schmucki, G., Brozova, N., Bühler, Y., 2021. Avalanche Protection Forest: From Process Knowledge to Interactive Maps. IntechOpen. https://doi.org/10.5772/intechopen.99514.
Bentz, B.J., Régnière, J., Fettig, C.J., Hansen, E.M., Hayes, J.L., Hicke, J.A., Kelsey, R.G., Negrón, J.F., Seybold, S.J., 2010. Climate Change and Bark Beetles of the Western United States and Canada: Direct and indirect Effects. Bioscience 60, 602–613. https://doi.org/10.1525/bio.2010.60.8.6.
Berger, F., Rey, F., 2004. Mountain protection forests against natural hazards and risks: New french developments by integrating forests in risk zoning. Nat. Hazards 33, 395–404. https://doi.org/10.1023/B:NHAZ.0000048468.67886.e5.
Brang, P., Schönenberger, W., Ott, E., Gardner, B., 2001. Forests as protection from natural hazards. In: The Forests Handbook. Wiley-Blackwell Publishing Ltd, pp. 53–81. https://doi.org/10.1002/9780470757079.ch3.
Brasington, J., Langham, J., Rumsby, B., 2003. Methodological sensitivity of morphometric estimates of coarse fluvial sediment transport. Geomorphology 53, 299–316. https://doi.org/10.1016/S0169-555X(02)00320-3.
Brovelli, M.A., Cannata, M., Longoni, U.M., 2004. LIDAR Data Filtering and DTM Interpolation within GRASS. Trans. GIS 8, 155–174. https://doi.org/10.1111/j.1467-9671.2004.00173.x.
Brožová, N., Fischer, J.-T., Bühler, Y., Bartelt, P., Bebi, P., 2020. Determining forest parameters for avalanche simulation using remote sensing data. Cold Reg. Sci. Technol. 172, 102976 https://doi.org/10.1016/j.coldregions.2019.102976.
Brožová, N., Baggio, T., D'Agostino, V., Bühler, Y., Bebi, P., 2021. Multiscale analysis of surface roughness for the improvement of natural hazard modelling. Nat. Hazards Earth Syst. Sci. 21, 3539–3562. https://doi.org/10.5194/nhess-21-3539-2021.
Bühler, Y., Kumar, S., Veitinger, J., Christen, M., Stoffel, A., 2013. Automated identification of potential snow avalanche release areas based on digital elevation models. Nat. Hazards Earth Syst. Sci. 13, 1321–1335. https://doi.org/10.5194/nhess-13-1321-2013.
Bühler, Y., Bebi, P., Christen, M., Margreth, S., Stoffel, L., Stoffel, A., Marty, C., Schmucki, G., Caviezel, A., Kühne, R., Wohlwend, S., Bartelt, P., 2022. Automated avalanche hazard indication mapping on state wide scale. Nat Hazards Earth Syst Sci Discuss 1–22.
Burt, A., Disney, M., Calders, K., 2019. Extracting individual trees from lidar point clouds using treeseg. Methods Ecol. Evol. 10, 438–445. https://doi.org/10.1111/2041-210X.13121.
Caduff, M.E., Brožová, N., Kupferschmid, A.D., Krumm, F., Bebi, P., 2022. How large-scale bark beetle infestations influence the protective effects of forest stands against avalanches: a case study in the Swiss Alps. For. Ecol. Manag. 514, 120201 https://doi.org/10.1016/j.foreco.2022.120201.
Chandler, K.R., Stevens, C.J., Binley, A., Keith, A.M., 2018. Influence of tree species and forest land use on soil hydraulic conductivity and implications for surface runoff generation. Geoderma 310, 120–127. https://doi.org/10.1016/j.geoderma.2017.08.011.
Chirici, G., Giannetti, F., Travaglini, D., Nocentini, S., Francini, S., D'Amico, G., Calvo, E., Fasolini, D., Broll, M., Maistrelli, F., Tonner, J., Pietrogiovanna, M., Oberlechner, K., Andriolo, A., Comino, R., Faidiga, A., Pasutto, I., Carraro, G., Zen, S., Contarin, F., Alfonsi, L., Wolynski, A., Zanin, M., Gagliano, C., Tonolli, S., Zoanetti, R., Tonetti, R., Cavalli, R., Lingua, E., Pirotti, F., Grigolato, S., Bellingeri, D., Zini, E., Gianelle, D., Dalponte, M., Pompei, E., Stefani, A., Motta, R., Morresi, D., Garbarino, M., Alberti, G., Valdevit, F., Tomelleri, E., Torresani, M., Tonon, G., Marchi, M., Corona, P., Marchetti, M., 2019. Forest damage inventory after the "Vaia" storm in Italy. For - Riv di Selvic ed Ecol For 16, 3–9. https://doi.org/10.3832/efor3070-016.
Colomina, I., Molina, P., 2014. Unmanned aerial systems for photogrammetry and remote sensing: a review. ISPRS J. Photogramm. Remote Sens. https://doi.org/10.1016/j.isprsjprs.2014.02.013.
Dassot, M., Constant, T., Fournier, M., 2011. The use of terrestrial LiDAR technology in forest science: Application fields, benefits and challenges. Ann. For. Sci. 68, 959–974. https://doi.org/10.1007/s13595-011-0102-2.
Doneus, M., Briese, C., 2011. Airborne Laser Scanning in forested areas–potential and limitations of an archaeological prospection technique. In: Remote Sensing for Archaeological Heritage…, pp. 59–76.
Dorren, L.K.A., Berger, F., Le Hir, C., Mermin, E., Tardif, P., 2005. Mechanisms, effects and management implications of rockfall in forests. For. Ecol. Manag. 215, 183–195. https://doi.org/10.1016/j.foreco.2005.05.012.
Ellenberg, H., Leuschner, C., 2010. Vegetation Mitteleuropas mit den Alpen: in ökologischer [dynamischer und historischer Sicht].
Feistl, T., Bebi, P., Dreier, L., Hanewinkel, M., Bartelt, P., Bebi, P., Dreier, L., Hanewinkel, M., Bartelt, P., 2014. Quantification of basal friction for technical and silvicultural glide-snow avalanche mitigation measures. Nat. Hazards Earth Syst. Sci. 14, 2921–2931. https://doi.org/10.5194/nhess-14-2921-2014.
Frehner, M., Wasser, B., Schwitter, R., 2005. Nachhaltigkeit und Erfolgskontrolle im Schutzwald.Wegleitung für Pflegemassnahmen in Wäldern mit Schutzfunktion [Sustainability and controlling in protection forests. Guidelines for tending forests with protective function]. In: Bundesamt Für Umwelt. Wald Und Landschaft (BUWAL), Bern, Switzerland, p. 554.
Frey, W., Thee, P., 2002. Avalanche protection of windthrow areas: a ten year comparison of cleared and uncleared starting zones. Forest Snow Landscape Res. 77 (2), 89–107.
Gardiner, B., Blennow, K., Carnus, J.-M., Fleischer, P., Ingemarson, F., Landmann, G., Lindner, M., Marzano, M., Nicoll, B., Orazio, C., Peyron, J.-L., Reviron, M.-P., Schelhaas, M.-J., Schuck, A., Spielmann, M., Usbeck, T., 2010. Destructive Storms in European Forests: Past and Forthcoming Impacts.
Germain, D., Filion, L., Hétu, B., 2005. Snow avalanche activity after fire and logging disturbances, northern Gaspé Peninsula, Quebec. Canada Can J Earth Sci 42, 2103–2116. https://doi.org/10.1139/e05-087.
Getzner, M., Gutheil-Knopp-Kirchwald, G., Kreimer, E., Kirchmeir, H., Huber, M., 2017. Gravitational natural hazards: Valuing the protective function of Alpine forests. For Policy Econ 80, 150–159. https://doi.org/10.1016/j.forpol.2017.03.015.
Grohmann, C.H., Smith, M.J., Riccomini, C., 2011. Multiscale analysis of topographic surface roughness in the Midland Valley. Scotland IEEE Trans Geosci Remote Sens 49, 1200–1213. https://doi.org/10.1109/TGRS.2010.2053546.
Hegg, C., Badoux, A., Witzig, J., Lueser, P., 2005. Forest influence on flood runoff generation studied on the Sperbelgraben example. In: Progress in Surface and Subsurface Water Studies at Plot and Small Basin Scale, pp. 47–52.
Lingua, E., Bettella, F., Pividori, M., Marzano, R., Garbarino, M., Piras, M., Kobal, M., Berger, F., 2020. The Protective role of forests to reduce rockfall risks and impacts in the alps under a climate change perspective. In: Climate Change, Hazards and Adaptation Options. Springer, pp. 333–347. https://doi.org/10.1007/978-3-030-37425-9_18.
Maggioni, M., Gruber, U., 2003. The influence of topographic parameters on avalanche release dimension and frequency. Cold Reg. Sci. Technol. 37, 407–419. https://doi.org/10.1016/S0165-232X(03)00080-6.
May, C.L., 2002. Debris flows through different forest age classes in the Central Oregon Coast Range. J. Am. Water Resour. Assoc. 38 (4), 1097–1113.
McClung, D.M.M., 2001. Characteristics of terrain, snow supply and forest cover for avalanche initiation caused by logging. Ann. Glaciol. 32, 223–229.
McClung, D., Schaerer, P., 2006. The Avalanche Handbook.
Meyer-Grass, M., 1987. Waldlawinen: Gefährdete Bestände, Massnahmen, Pflege des Gebirgswaldes. In: Pflege Des Gebirgswaldes: Leitfaden Fur Die Begrünung Und Forstliche Nutzung von Gebirgswäldern. Bischoff, N, Bern, Switzerland.
Michelini, T., Bettella, F., D'Agostino, V., 2017. Field investigations of the interaction between debris flows and forest vegetation in two Alpine fans. Geomorphology 279, 150–164. https://doi.org/10.1016/j.geomorph.2016.09.029.
Mkaouar, A., Kallel, A., Guidara, R., Ben Rabah, Z., 2018. Detection of forest strata volume using LiDAR data. In: 4th International Conference on Advanced Technologies for Signal and Image Processing (ATSIP). IEEE, pp. 1–6. https://doi.org/10.1109/ATSIP.2018.8364496.
Moeser, D., Stähli, M., Tobias, J., 2015. Improved snow interception modeling using canopy parameters derived from airborne LiDAR data. Water Resour. Assoc. 51, 5041–5059. https://doi.org/10.1111/j.1752-1688.1969.tb04897.x.
Motta, R., Ascoli, D., Corona, P., Marchetti, M., Vacchiano, G., 2018. Silviculture and wind damages. The storm "Vaia.". For. - Riv. di Selvic. ed Ecol. For. 15, 94–98. https://doi.org/10.3832/efor2990-015.
Niculiță, M., 2020. Geomorphometric methods for burial mound recognition and extraction from high-resolution LiDAR DEMs. Sensors 20, 1192. https://doi.org/10.3390/s20041192.
Olmedo, I., Bourrier, F., Berger, Frédéric, Limam, A., Bertrand, D., Lollino, G., Giordan, D., Crosta, G.B., Corominas, J., Azzam, R., Wasowski, J., Sciarra, N., Berger, Frederic, 2015. Felled Trees as a Rockfall Protection System: Experimental and Numerical Studies Felled Trees as a Rockfall Protection System: Experimental and Numerical studies Felled trees as a rockfall protection system: ex-perimental and numerical studies. Eng Geol Soc Territ 2, 1889–1893. https://doi.org/10.1007/978-3-319-09057-3_335ï.
Paine, R.T., Tegner, M.J., Johnson, E.A., 1998. Compounded perturbations yield ecological surprises. Ecosystems 16, 535–545.
Perzl, F., 2005. Beurteilung der Lawinen-Schutzwirkung des Waldes. BFW-Praxisinformation 8, 27–31.
Popescu, S.C., Wynne, R.H., 2004. Seeing the trees in the forest: using lidar and multispectral data fusion with local filtering and variable window size for estimating tree height. Photogramm. Eng. Remote. Sens. 70, 589–604. https://doi.org/10.14358/PERS.70.5.589.
Qi, W., Saarela, S., Armston, J., Ståhl, G., Dubayah, R., 2019. Forest biomass estimation over three distinct forest types using TanDEM-X InSAR data and simulated GEDI lidar data. Remote Sens. Environ. 232, 111283 https://doi.org/10.1016/j.rse.2019.111283.
Quine, C.P., Bell, P.D., 1998. Monitoring of windthrow occurrence and progression in spruce forests in Britain. For An Int J For Res 71, 87–97. https://doi.org/10.1093/forestry/71.2.87-a.
R Core Team, 2021. R: A Language and Environment for Statistical Computing [WWW Document]. R Found. Stat. Comput. URL. http://www.r-project.org (accessed 1.28.21).
Radtke, P.J., Amateis, R.L., Prisley, S.P., Copenheaver, C.A., Chojnacky, D.C., Pittman, J. R., Burkhart, H.E., 2009. Modeling production and decay of coarse woody debris in loblolly pine plantations. For. Ecol. Manag. 257, 790–799. https://doi.org/10.1016/j.foreco.2008.10.001.
Rammer, W., Brauner, M., Ruprecht, H., Lexer, M.J., 2015. Evaluating the effects of forest management on rockfall protection and timber production at slope scale. Scand. J. For. Res. 30, 719–731. https://doi.org/10.1080/02827581.2015.1046911.
Ringenbach, A., Bebi, P., Bartelt, P., Caviezel, A., 2021. The role of forest deadwood in rockfall protection. In: EGU2021, p. 10791.
Roussel, J.R., Auty, D., Coops, N.C., Tompalski, P., Goodbody, T.R.H., Meador, A.S., Bourdon, J.F., de Boissieu, F., Achim, A., 2020. lidR: an R package for analysis of Airborne Laser Scanning (ALS) data. Remote Sens. Environ. https://doi.org/10.1016/j.rse.2020.112061.
Rusu, R.B., Cousins, S., 2011. 3D is here: Point Cloud Library (PCL). Proc - IEEE Int Conf Robot Autom 11–14. https://doi.org/10.1109/ICRA.2011.5980567.
Saeki, M., Matsuoka, H., 1969. Snow-buried young forest trees growing on steep slopes. J Japanese Soc Snow Ice 31, 19–23. https://doi.org/10.5331/seppyo.31.19.

Sappington, J.M., Longshore, K.M., Thompson, D.B., 2007. Quantifying Landscape Ruggedness for Animal Habitat Analysis: a Case Study using Bighorn Sheep in the Mojave Desert. J. Wildl. Manag. 71, 1419–1426. https://doi.org/10.2193/2005-723.

Schaerer, P.A., 1977. Analysis of snow avalanche terrain. Can. Geotech. J. 14, 281–287. https://doi.org/10.1139/t77-034.

Scheidl, C., Heiser, M., Vospernik, S., Lauss, E., Frank, Perzl, Kofler, A., Kleemayr, K., Bettella, F., Lingua, E., Garbarino, M., Skudnik, M., Trappmann, D., Berger, F., 2020. Assessing the protective role of alpine forests against rockfall at regional scale. Eur. J. For. Res. 139, 969–980. https://doi.org/10.1007/s10342-020-01299-z.

Schiesser, H.H., Pfister, C., Bader, J., 1997. Winter storms in Switzerland north of the Alps 1864/1865-1993/1994. Theor. Appl. Climatol. 58, 1–19. https://doi.org/10.1007/BF00867428.

Schneebeli, M., Bebi, P., 2004. Snow and Avalanche Control. Encycl For Sci 397–402. https://doi.org/10.1016/B0-12-145160-7/00271-4.

Schönenberger, W., 2002a. Windthrow research after the 1990 storm Vivian in Switzerland: Objectives, study sites, and projects. For Snow Landsc Res 77, 9–16.

Schönenberger, W., 2002b. Post windthrow stand regeneration in Swiss mountain forests: the first ten years after the 1990 storm Vivian. For. Snow Landsc. Res. 77, 61–80.

Schönenberger, W., Noack, A., Thee, P., 2005. Effect of timber removal from windthrow slopes on the risk of snow avalanches and rockfall. For. Ecol. Manag. 213, 197–208. https://doi.org/10.1016/j.foreco.2005.03.062.

Schweizer, J., Jamieson, J.B., Schneebeli, M., 2003. Snow avalanche formation. Rev. Geophys. 41 https://doi.org/10.1029/2002RG000123.

Seidl, R., Schelhaas, M.J., Lexer, M.J., 2011. Unraveling the drivers of intensifying forest disturbance regimes in Europe. Glob. Chang. Biol. 17, 2842–2852. https://doi.org/10.1111/j.1365-2486.2011.02452.x.

Seidl, R., Rammer, W., Spies, T.A., 2014a. Disturbance legacies increase the resilience of forest ecosystem structure, composition, and functioning. Ecol. Appl. 24, 2063–2077. https://doi.org/10.1890/14-0255.1.

Seidl, R., Schelhaas, M.J., Rammer, W., Verkerk, P.J., 2014b. Increasing forest disturbances in Europe and their impact on carbon storage. Nat. Clim. Chang. 4, 806–810. https://doi.org/10.1038/nclimate2318.

Seidl, R., Thom, D., Kautz, M., Martin-Benito, D., Peltoniemi, M., Vacchiano, G., Wild, J., Ascoli, D., Petr, M., Honkaniemi, J., Lexer, M.J., Trotsiuk, V., Mairota, P., Svoboda, M., Fabrika, M., Nagel, T.A., Reyer, O., 2017. Forest disturbances under climate change. Nat. Clim. Chang. 7, 395–402. https://doi.org/10.1038/NCLIMATE3303.

Silva, C.A., Hudak, A.T., Vierling, L.A., Loudermilk, E.L., O'Brien, J.J., Hiers, J.K., Jack, S.B., Gonzalez-Benecke, C., Lee, H., Falkowski, M.J., Khosravipour, A., 2016. Imputation of Individual Longleaf Pine (Pinus palustris Mill.) tree Attributes from Field and LiDAR Data. Can. J. Remote. Sens. 42, 554–573. https://doi.org/10.1080/07038992.2016.1196582.

Swanson, R.H., Stevenson, D.R., 1979. Managing snow accumulation and melt under leafless aspen to enhance watershed value. In: 39th Annual Western Snow Conference, pp. 63–69.

Teich, M., Fischer, J.T., Feistl, T., Bebi, P., Christen, M., Grêt-Regamey, A., 2014. Computational snow avalanche simulation in forested terrain. Nat. Hazards Earth Syst. Sci. 14, 2233–2248. https://doi.org/10.5194/nhess-14-2233-2014.

Teich, M., Giunta, A.D., Hagenmuller, P., Bebi, P., Schneebeli, M., Jenkins, M.J., 2019. Effects of bark beetle attacks on forest snowpack and avalanche formation – Implications for protection forest management. For. Ecol. Manag. 438, 186–203. https://doi.org/10.1016/j.foreco.2019.01.052.

Viglietti, D., Letey, S., Motta, R., Maggioni, M., Freppaz, M., 2010. Snow avalanche release in forest ecosystems: a case study in the Aosta Valley Region (NW-Italy). Cold Reg. Sci. Technol. 64, 167–173. https://doi.org/10.1016/j.coldregions.2010.08.007.

Wohlgemuth, T., Schwitter, R., Bebi, P., Sutter, F., Brang, P., 2017. Post-windthrow management in protection forests of the Swiss Alps. Eur. J. For. Res. 136, 1029–1040. https://doi.org/10.1007/s10342-017-1031-x.

Zhang, W., Qi, J., Wan, P., Wang, H., Xie, D., Wang, X., Yan, G., 2016. An easy-to-use airborne LiDAR data filtering method based on cloth simulation. Remote Sens. 8, 501. https://doi.org/10.3390/rs8060501.

Zhao, K., Suarez, J.C., Garcia, M., Hu, T., Wang, C., Londo, A., 2018. Utility of multitemporal lidar for forest and carbon monitoring: tree growth, biomass dynamics, and carbon flux. Remote Sens. Environ. 204, 883–897. https://doi.org/10.1016/j.rse.2017.09.007.